

J. R. Lukes

Graduate Student Researcher,
e-mail: jennifer@newton.me.berkeley.edu

D. Y. Li

Graduate Student Researcher,
e-mail: deyuli@newton.me.berkeley.edu

Department of Mechanical Engineering,
University of California,
Berkeley, CA 94720-1740

X.-G. Liang

Professor,
Department of Engineering Mechanics,
Tsinghua University,
Beijing 100084, China
e-mail: liangxg@tsinghua.edu.cn

C.-L. Tien

Hon. Mem. ASME
University Professor and NEC Distinguished
Professor of Engineering,
University of California,
Berkeley, CA 94720-1740
e-mail: nancie@uclink4.berkeley.edu

Molecular Dynamics Study of Solid Thin-Film Thermal Conductivity

This study uses the molecular dynamics computational technique to investigate the thermal conductivity of solid thin films in the direction perpendicular to the film plane. In order to establish a benchmark reference, the computations are based on the widely used Lennard-Jones argon model due to its agreement with experimental liquid-phase data, its physically meaningful parameters, and its simple two-body form. Thermal conductivity increases with film thickness, as expected from thin-film experimental data and theoretical predictions. The calculated values are roughly 30 percent higher than anticipated. Varying the boundary conditions, heat flux, and lateral dimensions of the films causes no observable change in the thermal conductivity values. The present study also delineates the conditions necessary for meaningful thermal conductivity calculations and offers recommendations for efficient simulations. This work shows that molecular dynamics, applied under the correct conditions, is a viable tool for calculating the thermal conductivity of solid thin films. More generally, it demonstrates the potential of molecular dynamics for ascertaining microscale thermophysical properties in complex structures.

[S0022-1481(00)02303-3]

Keywords: Conduction, Heat Transfer, Molecular Dynamics, Nanoscale, Thin Films

Introduction

Novel materials such as buckyballs and buckytubes, highly porous and ultrathin films, and quantum wires and dots are forming the building blocks of an exciting new world of submicron devices. For instance, solid thin films with characteristic dimensions from tens to hundreds of nanometers are key components in integrated-circuit transistors and quantum-well lasers. Device performance in these applications is very sensitive to operating temperature. Overheating in semiconductor lasers, for example, is a major obstacle to increased output power and integration ([1]). For the best design of micro and nanodevices and thin-film materials, knowledge of thermophysical properties such as thermal conductivity is of paramount importance.

It is well known from measurements on thin films that such materials display markedly lower thermal conductivities than their bulk counterparts. Several approaches exist to predict the thin-film thermal conductivity for materials where heat conduction by quantized lattice vibrations, or phonons, is dominant. These approaches include kinetic theory, the Boltzmann transport equation, and the Monte Carlo computational technique. Such methods, however, can have difficulty handling the nonuniformly distributed impurities, voids, cracks, dislocations, and complex geometries present in real films. Numerous studies, for example, that of Inoue et al. [2] show that the molecular dynamics technique is well suited for the study of nanoscale phenomena in solid-phase materials. Molecular dynamics is a computational method that simulates the real behavior of materials and calculates physical properties of these materials by simultaneously solving the equations of motion for a system of atoms interacting with a given potential. This method provides a needed supplement to experimental measurements, which can be extremely difficult at such length scales.

Despite the technological importance of solid thin films in thermally sensitive applications, no molecular dynamics calculation of the thermal conductivity of solid thin films as a function of thickness has been reported before. Related studies, however, have been made. Mountain and MacDonald ([3]) calculated the temperature dependence of thermal conductivity for two and three-dimensional 1000-particle solid films. Kaburaki and Machida [4] found that increasing the number of particles in a one-dimensional chain increases thermal conductivity. Kotake and Wakuri [5] showed for a two-dimensional solid system subjected to a constant flux that the resultant temperature gradients sharply increase as the system width is decreased. Recent work by Volz and Chen [6] indicates that solid nanowires exhibit a strong reduction in thermal conductivity as compared to the bulk.

Model of Argon-Type Solid Thin Films

Using the molecular dynamics technique in a three-dimensional computational domain, the current paper calculates thermal conductivity in a solid argon-type model system as the thickness in one dimension is varied. Although argon is not a real thin-film material, it is the best choice for an initial thin-film thermal conductivity molecular dynamics study. One important reason for this is the availability of a good intermolecular potential for argon. The widely accepted Lennard-Jones 12-6 (LJ) potential matches experimental data for bulk fluid argon reasonably well, employs meaningful physical constants as parameters, and possesses a simple, two-body form which requires much less computation time than more complex potentials involving three-body and higher terms ([7]). A rigorous quantum-mechanical approach is at present not feasible for systems of more than a few atoms because such a method is too numerically intensive. The efforts of many workers, for example, Car [8], are currently directed toward this problem.

Additional reasons for using the LJ potential to study solid thin films are that the results can be benchmarked against the large

Contributed by the Heat Transfer Division for publication in the JOURNAL OF HEAT TRANSFER. Manuscript received by the Heat Transfer Division, Feb. 28, 1999; revision received, Mar. 1, 2000. Associate Technical Editor: D. Poulikakos.

body of existing work on argon-type systems and that the argon model, as noted by Kristensen et al. [9], should reveal fundamental phenomena not only for argon but for a wide variety of materials. Also, the argon model, unlike models of more technologically relevant materials, should span from the microscale regime to the bulk regime in a reasonable computational domain size due to its short phonon mean free path.

After establishing a firm foundation for pure thin films, the argon model can then be extended to thin-film systems with impurities, pores, defects, and other types of complicated structures. To get the most quantitatively accurate results for a given material, a potential specific to that material should be used, but to predict qualitative trends, which is the aim of this paper, the argon model is a sensible choice.

Computational Procedure

Several molecular dynamics approaches can be used to calculate thermal conductivity [10]. The nonhomogeneous nonequilibrium approach was chosen for the present work because it provides a direct physical representation of heat flow in a thin film. A new nonhomogeneous nonequilibrium program, based on the equilibrium classical molecular dynamics subroutines of Allen and Tildesley [7], was written and used for all simulations.

The general approach of the program is to apply a constant heat flux to an argon-type solid system, calculate the resulting temperature gradient, and determine the thermal conductivity by a simple ratio of flux to temperature gradient. The reverse method, in which the system boundaries are kept at constant temperatures and the resultant flux is calculated, was initially tried. This was abandoned in favor of the current scheme due to the slow convergence of the heat flux value. The execution of the program proceeds as follows. First, the simulation cell is constructed of face-centered cubic unit cells. Each unit cell contains four atoms and corresponds to two atomic planes of atoms. Each atom is assigned a type according to its spatial position: “hot,” “cold,” “regular,” or “fixed.” The configuration of the simulation cell depends upon whether bulk (Fig. 1(a)) or perpendicular (Fig. 1(b)) conductivity is to be calculated. Bulk materials are simulated by using periodic boundary conditions, in which the actual simulation cell of a small number of atoms is essentially repeated infinitely in all three coordinate directions. A drawback of this method is that it suppresses phonons in solids with wavelengths larger than the simulation cell size ([7]).

For thin films, periodic boundary conditions are used in two coordinate directions. Fixed atoms, which remain at their lattice positions for the entire simulation, are usually used in the third, “thin” direction to enforce an adiabatic boundary condition. In some simulations, a free boundary condition was used in the thin direction. For these cases, the flux and initial temperature values had to be lowered to prevent evaporation of the surface atoms, and much longer simulations had to be run to reach steady state. Following the example of Kotake and Wakuri [5], four planes of fixed atoms are deemed sufficient to simulate an infinite wall due to the short range of the interatomic forces. All nonfixed atoms are given an initial temperature by choosing their velocities according to the Maxwell distribution at that temperature. After this, the program advances the difference equations of motion for a short equilibration period to allow a realistic thermodynamic state to be established.

The difference equations come from the widely used “velocity Verlet” algorithm ([11]). In this algorithm, new atomic positions are calculated based on old positions, velocities, and forces. Velocities are calculated using a two-step scheme, in which old forces are used to advance old velocities to “half-step” velocities, new forces are calculated from the LJ potential using the new positions, and new velocities are found using the half-step velocities and new forces. The LJ potential is

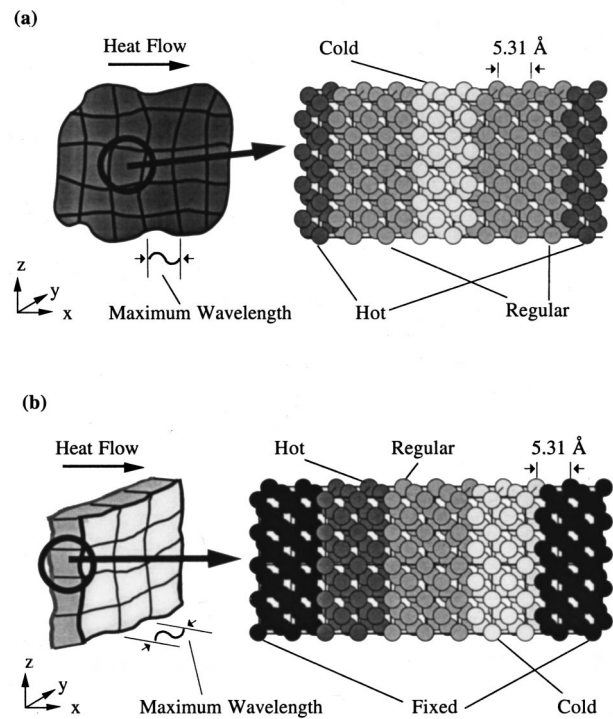


Fig. 1 Simulation cell schematic drawings: (a) bulk thermal conductivity, (b) perpendicular thermal conductivity

$$\phi_{LJ}(r_{ij}) = 4\epsilon_{LJ} \left\{ \left(\frac{\sigma_{LJ}}{r_{ij}} \right)^{12} - \left(\frac{\sigma_{LJ}}{r_{ij}} \right)^6 \right\}. \quad (1)$$

Only the neighbors of an atom within a certain cutoff radius, $2.6\sigma_{LJ}$, are included in the force calculations because faraway atoms have a negligible contribution to the total force on a given atom. This molecular dynamics convention keeps computation time manageable.

After equilibration, a heat flux is imposed on the system by adding a fixed amount of energy to hot atoms and removing the same amount of energy from cold atoms at every time step. This induces heat flow in the x -direction from the hot region to the cold region across the regular atoms. The algorithm of Ikeshoji and Hafskjold [12], which is used to apply the flux, alters kinetic energy in the hot region by scaling each hot atom’s velocity by the same factor R and by subtracting the same small velocity v_{sub} from this scaled velocity. The values of R and v_{sub} , which change at each time step, are chosen to conserve momentum and to add the desired amount of energy. A similar procedure is followed for the cold atoms, except kinetic energy is subtracted rather than added.

Instantaneous temperatures in each atomic x -plane are calculated using the formula

$$T_l = m \sum_{i=1}^{N_l} v_i^2 / 3N_l k_B \quad (2)$$

where the squares of the magnitudes of the atomic velocities in a particular plane are summed in accordance with the equipartition principle. The time-averaged temperature, standard deviation of temperature, and standard error of temperature are then calculated for each plane. The standard error of the planar temperature [13,7]

$$\sigma_{\langle T_l \rangle} = \sigma_{T_l} \sqrt{2\tau_{corr} / \tau_{run}} \quad (3)$$

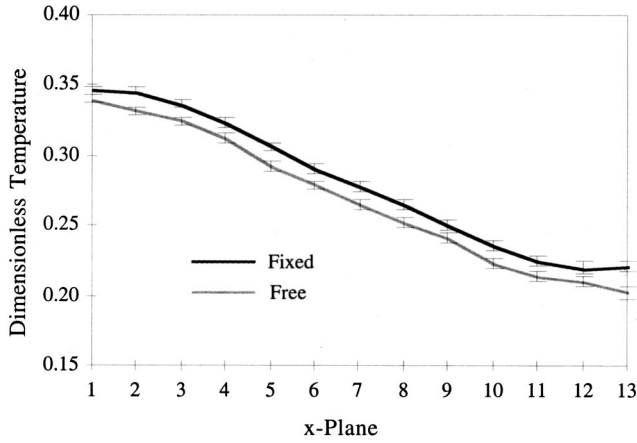


Fig. 2 Temperature in each x -plane of a five regular plane simulation for fixed and free boundaries

depends on the simulation run time at steady state and on the characteristic time over which the instantaneous planar temperatures are self-correlated. For simplicity, it is assumed that

$$\tau_{\text{corr}} \approx \text{MFP}/v_s, \quad (4)$$

$$\sigma_b = \sqrt{\left(\sum_{l=1}^p \frac{1}{\sigma_{\langle T_l \rangle}^2} \right) / \left[\left(\sum_{l=1}^p \frac{1}{\sigma_{\langle T_l \rangle}^2} \right) \left(\sum_{l=1}^p \frac{l^2}{\sigma_{\langle T_l \rangle}^2} \right) - \left(\sum_{l=1}^p \frac{l}{\sigma_{\langle T_l \rangle}^2} \right)^2 \right]} \quad (6)$$

are found using a weighted least-squares method ([18]).

Finally, thermal conductivity is found from

$$k = -a q_{\text{eff}} / 2b \quad (7)$$

where the factor $a/2$ accounts for the fact that the plane spacing is one-half the lattice parameter. Note that q_{eff} is not exactly the same as the ideal imposed heat flux due to small nonzero fluxes that occur in the y and z -directions. The actual heat flux through each regular plane is calculated from particle positions and velocities at regular intervals throughout the simulation using the equations of Irving and Kirkwood [19], and the time averages of these planar calculated fluxes are then spatially averaged over the regular planes

$$q_{\text{eff}} = \left(\sum_{l=1}^p \frac{\langle q_l \rangle}{\sigma_{\langle q_l \rangle}^2} \right) / \left(\sum_{l=1}^p \frac{1}{\sigma_{\langle q_l \rangle}^2} \right) \quad (8)$$

to yield effective flux. The standard error of planar flux is calculated as above for temperature in Eq. (3), and its squared reciprocal is used as the weighting factor in Eq. (8). For each simulation, the expression for error propagation in Press et al. [18] is used to calculate the probable error of effective flux

$$\sigma_{q_{\text{eff}}} = \sqrt{\sum_{l=1}^p \sigma_{\langle q_l \rangle}^2 \left(\frac{\partial q_{\text{eff}}}{\partial \langle q_l \rangle} \right)^2} \quad (9)$$

and is also used to find the probable error of thermal conductivity

$$\sigma_k = \sqrt{\sigma_{q_{\text{eff}}}^2 \left(\frac{\partial k}{\partial q_{\text{eff}}} \right)^2 + \sigma_b^2 \left(\frac{\partial k}{\partial b} \right)^2} \quad (10)$$

where the mean free path (MFP) in argon at the given planar temperature ([14,15]) and highest tabulated speed of sound for fluid argon from the CRC Handbook [16] are used. The fluid argon value was used because solid argon values were not available. The assumption of Eq. (4) is supported by the work of Volz et al. [17], who found good agreement between the autocorrelation time and the kinetic theory mean free time for molecular dynamics simulations on solid argon.

Figure 2 shows a pair of example temperature profiles; the magnitude of the standard error is indicated by the error bars. In this figure, the five regular atom x -planes in the center display a linear profile and the source (hot) and sink (cold) atoms on either side show the expected parabolic curvature. The slope of the best line fitted to the temperature profile of the regular atoms

$$b = \frac{\left(\sum_{l=1}^p \frac{1}{\sigma_{\langle T_l \rangle}^2} \right) \left(\sum_{l=1}^p \frac{l \langle T_l \rangle}{\sigma_{\langle T_l \rangle}^2} \right) - \left(\sum_{l=1}^p \frac{l}{\sigma_{\langle T_l \rangle}^2} \right) \left(\sum_{l=1}^p \frac{\langle T_l \rangle}{\sigma_{\langle T_l \rangle}^2} \right)}{\left(\sum_{l=1}^p \frac{1}{\sigma_{\langle T_l \rangle}^2} \right) \left(\sum_{l=1}^p \frac{l^2}{\sigma_{\langle T_l \rangle}^2} \right) - \left(\sum_{l=1}^p \frac{l}{\sigma_{\langle T_l \rangle}^2} \right)^2} \quad (5)$$

and the probable error of this slope

Results and Discussion

General Comments About Simulation. The simulations were run on DEC 3000 workstations, an AlphaServer 2000, and a Dell Optiplex GX1p PC running the Linux operating system. The numerical differences in results across the different platforms were negligible. Computation time varied from a few hours to several days, depending on the sizes of the systems considered. The total simulated time varied from tens of picoseconds to nanoseconds and was chosen to be proportional to the characteristic thermal diffusion time estimated for each system. Two types of thermal conductivity simulations were run: bulk and perpendicular. Critical input parameters for the simulations are listed in Table 1; other input parameters and detailed results for each simulation are listed elsewhere [20]. Standard LJ nondimensionalizations for temperature and thermal conductivity are used in the simulations:

Table 1 Simulation parameters

| Parameter | Value |
|--|----------------------------|
| LJ well depth parameter | 1.67×10^{-21} J |
| LJ equilibrium separation parameter | 3.4 Å |
| Argon atomic mass | 66.3×10^{-27} kg |
| Boltzmann's constant | 1.38×10^{-23} J/K |
| Lattice constant | 5.31 Å |
| Time step | 1 fs |
| Imposed dimensionless heat flux* | 1.0 |
| Cross-sectional unit cells* | 4 |
| Unit cells in each hot or cold region* | 2 |
| Unit cells in each fixed region | 2 |

*Parameters for specific simulations have been varied as noted in text.

$$T^* = \frac{k_B T}{\varepsilon_{LJ}} \quad k^* = k \frac{\sigma_{LJ}^2}{k_B} \sqrt{\frac{m}{\varepsilon_{LJ}}} \quad (11)$$

Since all parameters are dimensionless, the superscript will henceforth be dropped.

Two important criteria for the simulations are that q_{eff} is nearly the same as the imposed flux, and that the temperature profiles are reasonably close to linear. The profiles should not be expected to be completely linear, since thermal conductivity displays some temperature dependence. If the two criteria above are not satisfied, the thermal conductivity calculation, which is based on the Fourier law, is not valid. It was found that the typical reason that the criteria are not met is a too-short simulation time, although in very preliminary simulations lack of energy conservation due to a too-large time step and explosion of the lattice due to a too-small initial lattice spacing also occurred. It was observed that simulations not run long enough to attain a steady state yielded values of q_{eff} lower than the imposed fluxes and showed distinctly nonlinear temperature profiles. This is reasonable, since a finite time is required for the film to reach steady state after imposition of the heat flux at the boundaries. The flux discrepancies disappeared and the temperature profiles became more linear as the number of time steps in the simulation increased. Due to the difficulty in choosing a simulation time long enough to satisfy the criteria yet short enough to avoid undue computational burden, a trial-and-error process had to be followed to find values for τ_{run} . Values roughly 20 times the characteristic diffusion time were found sufficient to satisfy the criteria. For the thermal conductivity simulations reported here, the q_{eff} values were all within four percent of the ideal imposed flux and the temperature profiles were reasonably linear.

Momentum conservation, as expected, was found to hold exactly for the present 96 and 252-atom bulk simulations. In bulk simulations with more atoms, and in all thin-film simulations, however, the algorithm of Ikeshoji and Hafskjold [12] did not strictly conserve instantaneous total system momentum. Instead, the instantaneous momentum fluctuated rapidly about zero, the time-averaged system momentum value. The reason for this is not known, but is thought to be the result of small accumulated numerical errors due to roundoff and truncation of the potential at the cutoff radius. The standard deviation of the momentum fluctuations for the bulk and free-boundary thin-film simulations was several orders of magnitude smaller than that for fixed-boundary thin-film simulations, indicating that there may be some wall effect that works against momentum conservation. Considering that the wall atoms influence the motion of the regular, hot, and cold atoms without themselves being affected, in a manner analogous to a wall of infinite mass imparting impulses to impinging billiard balls, it is reasonable that momentum is not strictly conserved. Despite the lack of exact momentum conservation, no significant difference was found between the thermal conductivities for fixed and free-boundary simulations for both a 3 and a 5-regular plane case at a mean lattice temperature $T=0.27$ (Table 2). Thus, the observed small deviations from zero total momentum are not important for the purposes of this paper.

Table 2 Effect of boundary conditions on thermal conductivity

| Configuration | Thermal Conductivity | Error |
|--|----------------------|-------|
| Free boundary three regular planes | 0.391 | 0.075 |
| Fixed boundary three regular planes | 0.402 | 0.075 |
| Free boundary five regular planes | 0.474 | 0.051 |
| Fixed boundary five regular planes | 0.444 | 0.044 |

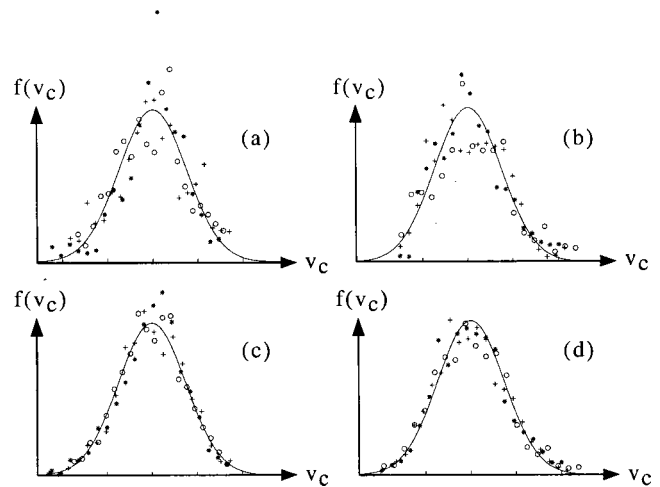


Fig. 3 Velocity distributions at $T=0.5$ for various cross sections and sampled time steps: (a) 4×4 , 10,000; (b) 6×6 , 10,000; (c) 4×4 , 30,000; (d) 6×6 , 30,000

Use of Eq. (2) to calculate planar temperature throughout the simulation assumes that a local thermodynamic equilibrium is established in each atomic plane. Tenenbaum et al. [21] and Hafskjold and Ratkje [22] assert that local thermodynamic equilibrium is established in molecular dynamics simulations of nonequilibrium fluids provided that the control volume thickness is roughly equal to the mean interatomic distance. If true for fluids, it is even more likely to be true for atomic planes in solids because the increased density causes increased interatomic interaction that aids interplanar energy transport. To test whether local thermodynamic equilibrium was established in the present case, the velocity of a single central atom in each regular, hot, and cold plane was monitored for the last 10,000 and 30,000 fs of a $T=0.5$ simulation of a thin film with seven regular planes. Two different values of cross section, or number of y unit cells by the unit of z unit cells, were used: 4×4 (32 atoms/plane) and 6×6 (72 atoms/plane). Figure 3 shows a histogram of the $x(o)$, $y(+)$, and $z(*)$ velocity components of the central atom for a representative regular plane along with the Maxwell distribution at the time-averaged planar temperature. The figure clearly shows that while there are some discrepancies between the Maxwell distribution and the calculated velocity distribution for the 10,000 cases, the 30,000 cases show much better agreement for both 4×4 and 6×6 cross sections. Since τ_{run} for all simulations is longer than 30,000 fs, it is reasonable to assume that the real calculated velocity distribution is even closer to a perfect Maxwellian. Increasing the cross section from 4×4 to 6×6 causes a much less dramatic improvement of the velocity distribution for both 10,000 and 30,000 at this temperature. This result suggests that longer simulations may be more effective than increased cross sections in attaining local thermodynamic equilibrium. The Maxwellian nature of the velocity distributions and the linear temperature profiles in the calculations indicate that the local thermodynamic equilibrium assumption is justified.

Bulk Thermal Conductivity. Bulk thermal conductivity was calculated for simulation cells of various sizes at dimensionless mean lattice temperatures of 0.3 and 0.5 to check the agreement of the model with experimental data for bulk solid argon. Mean lattice temperatures were found by spatially averaging the steady-state time-averaged temperatures of the regular atoms. Each data point in the $T=0.5$ case has a different cross section, increasing with the number of atoms from 2×2 to 8×8 . The conductivities at each temperature, normalized by the dimensionless experimental value corresponding to that temperature ([23]), are illustrated

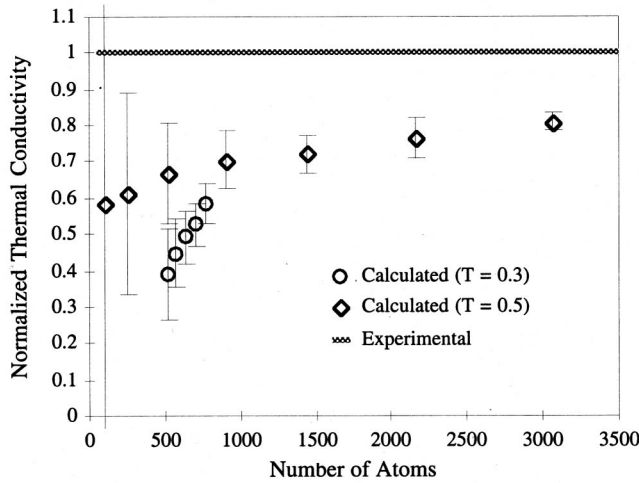


Fig. 4 Calculated and experimental bulk thermal conductivities at $T=0.3$ and 0.5 versus number of atoms

in Fig. 4. The error bars represent the normalized standard error of thermal conductivity (Eq. (10)) for each simulation.

For both temperatures, the calculated bulk thermal conductivity is observed to increase as the number of atoms is increased. The dependence of calculated macroscopic properties on the number of particles in a molecular dynamics simulation is a well-known artifact [24]. A recent example of the particle number dependence of bulk thermal conductivity can be found in Kaburaki et al.'s [25] calculation of solid bulk argon thermal conductivity for 256 and 500-atom systems, which shows a similar number dependence to that found in the present paper at comparable temperatures. The key to getting accurate bulk results from the molecular dynamics technique is to choose conditions that allow the finite simulation cell to represent, as closely as is feasible, an infinite bulk domain. True bulk-like behavior is indicated by minimal size dependence of the calculated values. Ideally, this could be accomplished by simulating a very large number of atoms, but in practice this is computationally quite burdensome.

It can be seen in Fig. 4 that the results at $T=0.3$, as compared to those at $T=0.5$, display a steeper number dependence and constitute a smaller portion of their corresponding bulk experimental value. This shows that for the same number of atoms, simulations run at higher temperatures better capture bulk behavior. A simple explanation for the more bulk-like behavior at higher temperatures is that the phonon mean free path is shorter, so the ratio of the mean free path to characteristic simulation cell dimension is smaller. In the bulk limit, this ratio is much less than 1.

Another interpretation is offered by the concept of phonon radiation ([26]). This concept, strictly valid in the ballistic limit of heat conduction in which the local thermodynamic equilibrium is not reached, can nevertheless offer some value in understanding the current results. Figure 5 thus uses the Planck formula ([27])

$$e(\lambda) = 2\pi C_1 / \lambda^5 (e^{C_2/\lambda T} - 1) \quad (12)$$

to estimate the spectral distribution for phonon "emissive power" under various conditions of temperature and computational domain size. Here the constants

$$C_1 = hv_s^2 \quad C_2 = hv_s/k_B \quad (13)$$

are defined using the speed of sound rather than the speed of light. Figures 5(a) and 5(b) show that for a given maximum allowed phonon wavelength, which is equal to the characteristic dimension of the simulation cell, raising the temperature increases the allowed phonon fraction due to the decreased peak phonon wavelength.

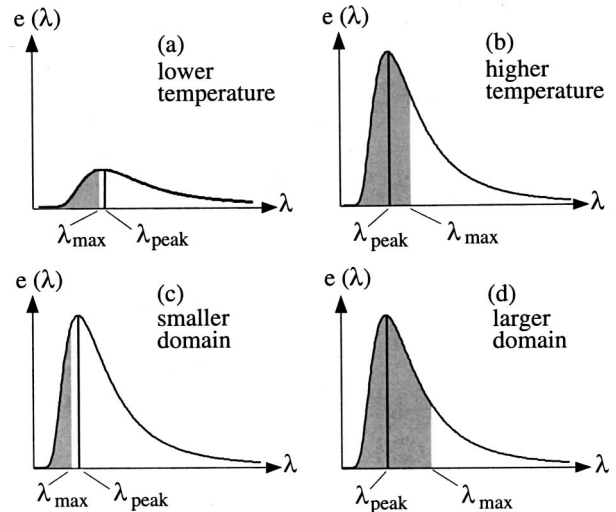


Fig. 5 Planck spectral distribution. Shaded areas indicate the fraction of total phonon emissive power allowed by the molecular dynamics simulation. (a) and (b) illustrate the effect of temperature, and (c) and (d) illustrate the effect of domain size.

The figures also suggest a guideline: $L/\lambda_{\text{peak}}(T)$ should be as much larger than 1 as possible. This will make the phonon fraction approach 1, ensuring that molecular dynamics simulations yield bulk-like results. A Wien's law formulation for phonons can be used to estimate $L/\lambda_{\text{peak}}(T)$. Taking the derivative of Eq. (12), iterating for C_2 , and substituting yields

$$\lambda_{\text{peak}} T \approx 0.2 \quad L/\lambda_{\text{peak}} \approx 5LT. \quad (14)$$

Increasing the computational domain size at a given temperature, as is shown going from Fig. 5(c) to Fig. 5(d), also increases the fraction allowed by the simulation. In the limit of infinite domain size the fraction becomes 1, but as discussed above, using higher temperatures is the most computationally economical choice.

A simulation cell size of 512 atoms, which corresponds to a system with eight regular x -planes of 4×4 cross section, yields thermal conductivity values at $T=0.5$ not much smaller than those with a significantly larger number of atoms. For computational efficiency it was thus assumed that four unit cells were adequate to represent infinite length in a particular direction. In

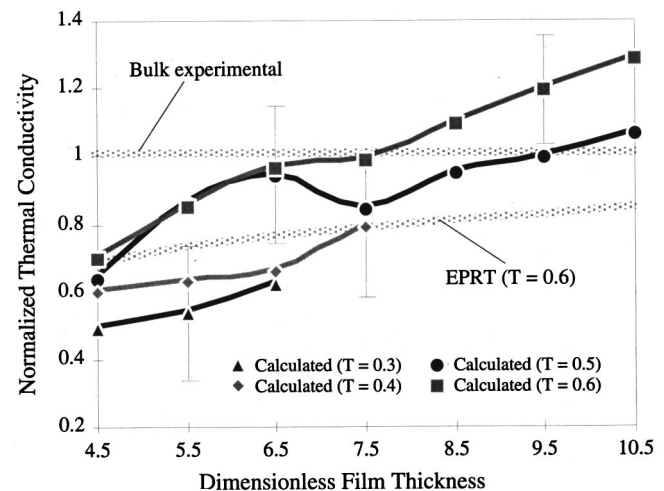


Fig. 6 Calculated, bulk experimental, and equation of photon radiative transfer (EPRT) thermal conductivities versus film thickness at various temperatures

the perpendicular thermal conductivity simulations of the following section, then, 4×4 cross sections were used to represent “infinite” length in the y and z -directions.

Perpendicular Thermal Conductivity. Figure 6 displays the calculation results for normalized perpendicular thermal conductivity versus dimensionless film thickness at several mean lattice temperatures. A thin film thermal conductivity estimate based on Majumdar’s equation of phonon radiative transfer ([28]) is shown for comparison. As in the bulk case, the results at each temperature are normalized by the experimental conductivity value at that temperature. For clarity, film thickness is nondimensionalized by a rather than by the typically used σ_{LJ} and only one error bar is shown for each set of temperature data. The error bar magnitude corresponds not to the actual calculated error at the corresponding thickness, but to the largest error of the set, which occurs at the dimensionless thickness 4.5 for all sets. A heat flux value of 1.5 was used in the $T=0.6$ case because the higher fluxes cause steady state to be reached sooner. Film thickness, which was varied by adding/subtracting atomic x -planes to/from the computational cell, corresponds to the thickness of the regular atoms plus the thickness of the three hot x -planes and the three cold x -planes nearest the regular atoms.

It is critically important to note that unlike the bulk simulations discussed above, which in the ideal case display little size/number dependence, thin film simulations *should* reveal thickness-dependent properties due to the effect of the boundaries. As the film thickness increases, the boundary effect should be less pronounced and the calculated results should approach the bulk thermal conductivity value. As anticipated, Fig. 6 shows that thermal conductivity at all temperatures increases with film thickness. The unexpected undulation of the $T=0.5$ curve is fully contained within the envelope of its error bars.

Four observations should be made from the calculated data. The first is that the conductivities of lower-temperature films constitute a smaller fraction of their corresponding bulk values than identically sized higher-temperature films. This is in agreement with the temperature trends displayed by the bulk results, and shows that thin-film size effects are more pronounced at lower temperatures. The second is that the molecular dynamics values for thermal conductivity at $T=0.6$, while showing the same trend as the equation of photon radiative transfer results at the same temperature, are higher in magnitude. This can be explained by the fact that the mean free path and v_s values used in Eq. (4) above were inserted into the equation of photon radiative transfer model. The mean free path, as estimated above, is only a ballpark figure, and v_s is undoubtedly on the low side since it is for high-density fluid argon.

The third observation is that while the expected behavior is an asymptotic increase of the thin film results toward the bulk value, the thicker films for the $T=0.5$ and 0.6 cases appear to have thermal conductivities that exceed their corresponding experimental bulk values. This discrepancy is about 30 percent for the $T=0.6$ case. Using a similar nonhomogeneous nonequilibrium method on a fluid argon system of comparable size to these thicker films, Ciccotti and Tenenbaum [29] calculated a bulk thermal conductivity 20 percent above the experimental value. A reason for these discrepancies could be the fact that experimental samples always contain impurities and imperfections that reduce thermal conductivity below its ideal maximum value. The “sample” in the simulation, in contrast, is a perfectly pure single crystal. As its thickness increases it is reasonable that the conductivity may at some point exceed the experimental value while still being lower than the ideal maximum value. Also, there is no obvious reduction in the rate of conductivity increase for the thicker films, whose maximum thickness 10.5 corresponds to about five times the mean free path. An explanation may be that the results affirm the validity of the criterion of Flik et al. [30], which holds that perpendicular thin film thermal conductivity size effects are important when the film thickness is smaller than seven times the

mean free path. Thicker films may need to be simulated in order to see unmistakable asymptotic behavior. On the other hand, it is possible that asymptotic behavior *is* occurring, and that it is simply obscured within the envelope of the error bars.

The fourth observation is that within error, the bulk thermal conductivities in Fig. 4 are the same as the $T=0.3$ and 0.5 thin-film conductivities for comparable x -direction thickness. This result was puzzling at first, because it contradicted the expectation that the calculated bulk values would always exceed calculated thin-film values even for comparable domain sizes. Phonon mode counting in solid state physics, however, indicates that periodic boundary conditions (bulk) and fixed end boundary conditions (thin film) yield the same number of phonon modes for the same number of atoms ([31]). This means that the abovementioned phonon fraction for similarly sized bulk and thin film configurations is similar, so the thermal conductivity will also be similar. There is nothing intrinsic about periodic boundary conditions that changes its value to differ from the thin film value. Support for this argument can also be found in Table 2, which illustrates the effect of free versus fixed boundary conditions on thin film thermal conductivity. The results imply that the thermal conductivity calculated in a molecular dynamics simulation is affected by the physical dimension of the film but not by the boundary conditions.

Effect of Varying Computational Parameters. To investigate the effect of the chosen parameters on the thin film molecular dynamics results, several simulations with differing values of these parameters were run. As discussed above, changing the boundary configuration has no effect on the calculated thermal conductivity. It does, however, influence the magnitude of the temperature profile. The fixed boundary profile is higher than the free boundary profile for both the 3 and 5-regular plane cases listed in Table 2. The profile for the 5-plane case is plotted in Fig. 2. The discrepancy in the temperature profiles is probably caused by the two percent expansion exhibited by the free-boundary film. Expansion causes an increase in the LJ potential energy, resulting in a decreased kinetic energy and thus a decreased temperature. Also, it can be seen from Fig. 2 that the adiabatic walls present in the fixed boundary case appear to have some moderating effect on the temperatures of the outermost hot and cold planes. Since the boundary condition simulations use a lower flux, it was also necessary to explore the influence of this parameter. Table 3 shows that varying the flux for a film with three regular planes at $T=0.5$ does not cause any significant change in thermal conductivity. The use of a different flux for the boundary condition simulations is thus unlikely to be the cause of any unusual effects.

Another parameter investigated in the simulations was the number of unit cells in each hot/cold region. The thickness of these “bath” regions was reduced to 1 unit cell from the usual value of 2 unit cells to see the effect on thermal conductivity. Figure 7 illustrates that bath regions do contribute to thermal conductivity, because decreasing their thickness decreases the conductivity value. This suggests that the thickness of the film should be defined not just in terms of the thickness of the regular atomic planes, but should also include the thickness of the bath atoms. Including the entire thickness of the bath regions in the length would effectively shift the two unit cells/bath curve (henceforth called “A”) two thickness units to the right relative to the one unit cell/bath curve (“B”). This, however, would cause a different discrepancy: the conductivity for B would be higher than that

Table 3 Effect of imposed flux on thermal conductivity

| Flux | Thermal Conductivity | Error |
|------|----------------------|-------|
| 0.6 | 0.699 | 0.144 |
| 1.0 | 0.731 | 0.149 |
| 1.4 | 0.683 | 0.095 |

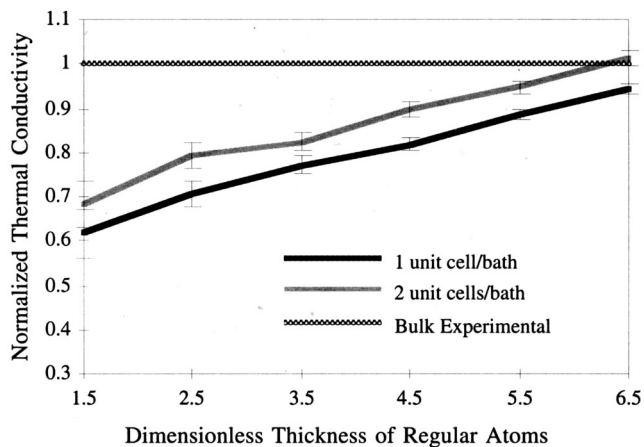


Fig. 7 Effect of number of unit cells per bath on thermal conductivity

for A. If only the first three hot and cold bath planes (1.5 unit cells) nearest the regular layers are included in the definition of film thickness rather than all four bath planes (2 unit cells) on each side, A shifts one thickness unit to the right and falls *directly* on top of B. This is the desired result, because the same thickness of atoms at the same temperature should necessarily produce the same calculated value of thermal conductivity. The fact that only three of the bath planes on either side appear to influence thermal conductivity is reasonable, since the cutoff radius $2.6\sigma_{LJ}$ corresponds to a thickness of 1.7 unit cells. The fourth plane is two unit cells away from the regular atoms and thus is too distant to interact with them. This also indicates that three planes of fixed atoms rather than four could be used to represent the fixed wall boundary condition.

The final parameter investigated was the cross section. Figure 8 shows thermal conductivity versus film thickness at $T=0.5$ for 4×4 and 6×6 cross sections. The error bars for the 4×4 case were made heavier than the 6×6 error bars for clarity. Within the error bars, the 6×6 case shows no discernible increase in thermal conductivity over the 4×4 case. Since large lateral dimensions were not necessary to obtain good thermal conductivity values, this result implies that the 4×4 case is large enough to capture the essential physics. Also, the unusual curvature discussed above for the 4×4 case disappears and the error bars shrink considerably. These two effects cannot be attributed to the increased cross section alone, however, because the steady-state simulation times

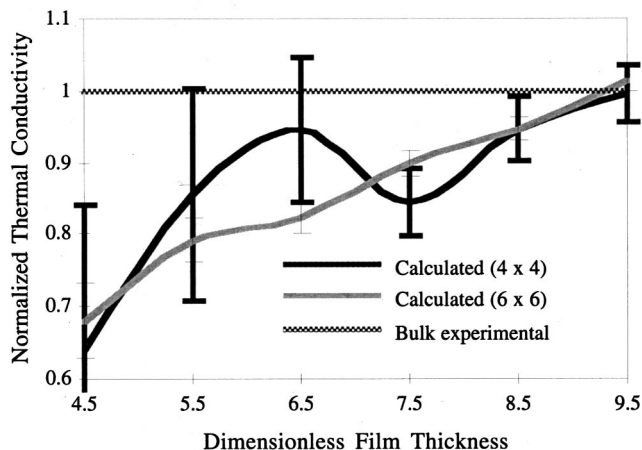


Fig. 8 Effect of cross section on thermal conductivity

Table 4 Effect of simulation time on thermal conductivity

| 4×4 τ_{run} , 6×6 τ_{run} , Configuration | τ_{run} Ratio | σ_k Ratio | Percentage due to τ_{run} Difference |
|--|--------------------|------------------|---|
| 32.9 ps, 260.0 ps 3 regular planes | 7.90 | 3.92 | 50% |
| 45.9 ps, 360.0 ps 5 regular planes | 7.84 | 4.87 | 62% |
| 61.1 ps, 400.0 ps 7 regular planes | 6.55 | 4.62 | 71% |
| 128.4 ps, 440.0 ps 9 regular planes | 3.43 | 2.63 | 77% |
| 147.9 ps, 440.0 ps 11 regular planes | 2.97 | 2.70 | 91% |
| 169.6 ps, 440.0 ps 13 regular planes | 2.59 | 2.43 | 94% |

used for the 6×6 runs were always longer than those for the 4×4 runs. Since σ_{T_i} in Eq. (3) is roughly inversely proportional to the square root of τ_{run} , it can be seen that the thermal conductivity error is approximately inversely proportional to τ_{run} . This can be used to estimate the effect of simulation time on error and to try to isolate the effect of cross section. The steady-state time ratio in Table 4 is found by dividing τ_{run} for the 6×6 case by that for the 4×4 case, and the thermal conductivity error ratio is found by dividing the error of the 4×4 case by that of the 6×6 case for the various film thicknesses at their corresponding steady-state simulation times. The percentage column divides the error ratio by the time ratio, and is an estimate of the percentage of the difference in error between the 4×4 and 6×6 cases that is due to differences in simulation time. Table 4 indicates that for large τ_{run} , most of the difference in error between 4×4 and 6×6 thermal conductivity results is attributable to the simulation time difference, while at small τ_{run} , the cross section difference appears to make some contribution to the difference in error. Increasing the cross section, increasing the number of time steps, or increasing both yields more precise thermal conductivity results. Longer simulation times are more desirable, however, since they are less computationally demanding than larger cross sections. As in the discussion of local thermodynamic equilibrium above, it is concluded that longer simulation times are the best way to obtain good thermal conductivity values from molecular dynamics simulations.

Concluding Remarks

This paper explores the thermal conductivity of solid systems in both bulk and thin-film configurations using the molecular dynamics computational technique. As expected, the argon model yields results close to experimental data for bulk materials and predicts increased thermal conductivity observed for thin-film materials as film thickness is increased. Modest overprediction of thermal conductivity observed for the thicker films is probably caused by the perfect purity of the idealized argon model used in the simulations. Normalized thermal conductivity is substantially reduced in the colder films, indicating that thin film effects are more pronounced at low temperatures. Bulk systems with larger characteristic lengths and higher temperatures show better agreement with experimental data than those with smaller values; mean free path and maximum phonon wavelength arguments are presented to explain this behavior. Changing the boundary conditions and the imposed fluxes in the thin film simulations produces no significant change in thermal conductivity.

Two important criteria for valid molecular dynamics simulations are that the calculated effective flux be nearly the same as the imposed flux and that the temperature profiles be reasonably close to linear. The following recommendations are suggested as computationally efficient ways to satisfy these criteria. First, the smallest cross section possible that yields reasonable conductivity

values should be used. Second, a good initial choice for τ_{run} is 20 times the characteristic thermal diffusion time. Third, to reduce the error for a particular simulation, simulation time should be increased rather than cross section. Fourth, if the exact value of temperature is not critical, simulations should be run at as high a temperature as is feasible. High fluxes are also desired because they too cause quicker attainment of steady state and better averaging. Finally, fixed boundary simulations should be used for thin films because they allow the stable simulation of a wide range of conditions.

This work has shown that molecular dynamics can be a powerful tool for predicting the thermal behavior of solid thin films. Future work should be done to apply this versatile, conceptually simple technique to microscale problems where other experimental and analytical approaches are difficult. The molecular dynamics technique is especially suited to study the thermophysical properties of disordered materials such as doped and nanoporous thin films and materials with voids, cracks, dislocations, or other complex geometries.

Acknowledgments

The authors gratefully acknowledge the financial support of the National Science Foundation.

Nomenclature

| | |
|-----------------------|--|
| a | = lattice constant |
| b | = slope of line fitted to temperature profile of regular atoms |
| C_1, C_2 | = constants in Planck formula |
| e | = phonon spectral "emissive power" |
| f | = distribution of x , y , or z -velocity component |
| h | = Planck's constant |
| k | = thermal conductivity |
| k_B | = Boltzmann's constant |
| L | = shortest characteristic simulation cell dimension |
| l | = particular regular atomic plane |
| MFP | = mean free path |
| m | = atomic mass |
| N_l | = number of atoms in plane l |
| p | = total number of regular atomic planes |
| q_{eff} | = effective heat flux in x -direction |
| $\langle q_l \rangle$ | = time-averaged actual heat flux in x -direction through plane l |
| R | = rescaling factor |
| r_{ij} | = distance between atoms i and j |
| T | = temperature |
| T_l | = temperature of plane l |
| $\langle T_l \rangle$ | = time-averaged temperature of plane l |
| v_c | = x , y , or z -velocity component |
| v_i | = velocity of atom i |
| v_s | = speed of sound |
| v_{sub} | = velocity subtracted from rescaled velocity |

Greek Symbols

| | |
|--------------------------------|--|
| ϵ_{LJ} | = Lennard-Jones well depth parameter |
| λ | = phonon wavelength |
| λ_{max} | = maximum phonon wavelength allowed by simulation domain |
| λ_{peak} | = peak phonon wavelength at a given temperature |
| σ_b | = probable error of slope |
| σ_k | = probable error of thermal conductivity |
| σ_{LJ} | = Lennard-Jones equilibrium separation parameter |
| $\sigma_{q_{\text{eff}}}$ | = probable error of effective flux |
| $\sigma_{\langle q_l \rangle}$ | = standard error of the time-averaged flux through plane l |
| σ_{T_l} | = standard deviation of the temperature of plane l |
| $\sigma_{\langle T_l \rangle}$ | = standard error of the time-averaged temperature of plane l |

| | |
|----------------------|---------------------------------------|
| τ_{corr} | = correlation time |
| τ_{run} | = steady state simulation run time |
| ϕ_{LJ} | = Lennard-Jones interatomic potential |

Superscript

* = dimensionless

References

- [1] Osinski, M., 1991, "Vertical-Cavity Surface-Emitting Semiconductor Lasers: Present Status and Future Prospects," *Proc. SPIE*, **1418**, pp. 2–24.
- [2] Inoue, R., Tanaka, H., and Nakanishi, K., 1996, "Molecular Dynamics Simulation Study of the Anomalous Thermal Conductivity of Clathrate Hydrates," *J. Chem. Phys.*, **104**, pp. 9569–9577.
- [3] Mountain, R. D., and MacDonald, R. A., 1983, "Thermal Conductivity of Crystals: A Molecular-Dynamics Study of Heat Flow in a Two-Dimensional Crystal," *Phys. Rev. B*, **28**, pp. 3022–3025.
- [4] Kaburaki, H., and Machida, M., 1993, "Thermal Conductivity in One-Dimensional Lattices of Fermi-Pasta-Ulam Type," *Phys. Lett. A*, **181**, pp. 85–90.
- [5] Kotake, S., and Wakuri, S., 1994, "Molecular Dynamics Study of Heat Conduction in Solid Materials," *J. Ser. B*, **37**, pp. 103–108.
- [6] Volz, S., and Chen, G., 1999, "Molecular Dynamics Simulation of Thermal Conductivity of Silicon Nanowires," *Appl. Phys. Lett.*, **75**, pp. 2056–2058.
- [7] Allen, M. P., and Tildesley, D. J., 1987, *Computer Simulation of Liquids*, Clarendon Press, Oxford, UK.
- [8] Car, R., 1996, "Modeling Materials by Ab-Initio Molecular Dynamics," *Quantum Theory of Real Materials*, Chelikowsky, J. R., and Louie, S. G., eds., Kluwer Academic, Dordrecht, The Netherlands, pp. 23–37.
- [9] Kristensen, W. D., Jensen, E. J., and Cotterill, R. M. J., 1974, "Thermodynamics of Small Clusters of Atoms: A Molecular Dynamics Simulation," *J. Chem. Phys.*, **60**, pp. 4161–4169.
- [10] Chou, F. C., Lukes, J. R., Liang, X. G., Takahashi, K., and Tien, C. L., 1999, "Molecular Dynamics in Microscale Thermophysical Engineering," *Ann. Rev. Heat Transf.*, **10**, pp. 141–176.
- [11] Swope, W. C., Andersen, H. C., Berens, P. H., and Wilson, K. R., 1982, "A Computer Simulation Method for the Calculation of Equilibrium Constants for the Formation of Physical Clusters of Molecules: Application to Small Water Clusters," *J. Chem. Phys.*, **76**, pp. 637–649.
- [12] Ikeshoji, T., and Hafskjold, B., 1994, "Non-equilibrium Molecular Dynamics Calculation of Heat Conduction in Liquid and through Liquid-Gas Interface," *Mol. Phys.*, **81**, pp. 251–261.
- [13] Jacucci, G., and Rahman, A., 1984, "Comparing the Efficiency of Metropolis Monte Carlo and Molecular Dynamics Methods for Configuration Space Sampling," *Nuovo Cimento*, **D4**, pp. 341–356.
- [14] Dobbs, E. R., and Jones, G. O., 1957, "Theory and Properties of Solid Argon," *Rep. Prog. Phys.*, **20**, pp. 516–564.
- [15] Dugdale, J. S., and MacDonald, D. K. C., 1955, "Lattice Thermal Conductivity," *Phys. Rev.*, **98**, pp. 1751–1752.
- [16] *CRC Handbook of Chemistry and Physics*, 1996, CRC Press, Boca Raton, FL.
- [17] Volz, S., Saulnier, J.-B., Lallemand, M., Perrin, B., Depondt, P., and Marschal, M., 1996, "Transient Fourier-law Deviation by Molecular Dynamics in Solid Argon," *Phys. Rev. B*, **54**, pp. 340–347.
- [18] Press, W. H., Teukolsky, S. A., Vetterling, W. T., and Flannery, B. P., 1992, *Numerical Recipes in FORTRAN: The Art of Scientific Computing*, 2nd Ed., Cambridge University Press, Cambridge, UK.
- [19] Irving, J. H., and Kirkwood, J. G., 1950, "The Statistical Mechanical Theory of Transport Processes. IV. The Equations of Hydrodynamics," *J. Chem. Phys.*, **18**, pp. 817–829.
- [20] Lukes, J. R., 2000, "Molecular Dynamics Simulation of Thermal Conduction in Thin Films and Nanoporous Materials," Ph.D. thesis, University of California, Berkeley, CA, in progress.
- [21] Tenenbaum, A., Ciccotti, G., and Gallico, R., 1982, "Stationary Nonequilibrium States by Molecular Dynamics," *Phys. Rev. A*, **25**, pp. 2778–2787.
- [22] Hafskjold, B., and Ratkje, S. K., 1995, "Criteria for Local Equilibrium in a System with Transport of Heat and Mass," *J. Stat. Phys.*, **78**, pp. 463–494.
- [23] Touloukian, Y. S., Liley, P. E., and Saxena, S. C., eds., 1970, *Thermal Conductivity: Nonmetallic Liquids and Gases*, IFI/Plenum, New York.
- [24] Haile, J. M., 1992, *Molecular Dynamics Simulation: Elementary Methods*, Wiley, New York.
- [25] Kaburaki, H., Li, J., and Yip, S., 1999, "Thermal Conductivity of Solid Argon by Classical Molecular Dynamics," *Mater. Res. Soc. Symp. Proc.*, **538**, pp. 503–508.
- [26] Casimir, H. B. G., 1938, "Note on the Conduction of Heat in Crystals," *Physica*, **5**, pp. 495–500.
- [27] Siegel, R., and Howell, J. R., 1981, *Thermal Radiation Heat Transfer*, 2nd Ed., Hemisphere, Washington, DC.
- [28] Majumdar, A., 1993, "Microscale Heat Conduction in Dielectric Thin Films," *ASME J. Heat Transfer*, **115**, pp. 7–16.
- [29] Ciccotti, G., and Tenenbaum, A., 1980, "Canonical Ensemble and Nonequilibrium States by Molecular Dynamics," *J. Stat. Phys.*, **23**, pp. 767–772.
- [30] Flik, M. I., Choi, B. I., and Goodson, K. E., 1992, "Heat Transfer Regimes in Microstructures," *ASME J. Heat Transfer*, **114**, pp. 666–674.
- [31] Kittel, C., 1996, *Introduction to Solid State Physics*, 7th Ed., Wiley, New York.